INAE Letters (2019) 4:241–250
https://doi.org/10.1007/s41403-019-00083-9

ORIGINAL ARTICLE

Effects of Strain Rate and Temperature on Tensile Properties, Deformation and Dynamic Strain Ageing Behavior of Ni-Base Superalloy Superni 263

Jhansi Jadav[1] · K. V. Rajulapati[1] · K. Bhanu Sankara Rao[2] · N. Eswara Prasad[3]

Received: 25 November 2019 / Accepted: 29 November 2019 / Published online: 19 December 2019

Abstract
Tensile studies on Superni 263 superalloy were carried out by employing various strain rates and temperatures in the range of (298–923 K), to explore the tensile deformation and fracture characteristics. It is found that Superni 263 alloy was sensitive to strain rate and peak value in yield strength was obtained at intermediate strain rate 1.3×10^{-3} S^{-1} and 673 K. The alloy exhibited serrated plastic flow, anomalous variations in tensile properties, minimum in ductility, work hardening rate and negative strain rate sensitivity which are the important manifestations of dynamic strain ageing (DSA) in the intermediate temperature range. The species responsible for the occurrence of DSA were identified as Cr and Mo with the activation energy measurements of 68–74 kJ/mol, indicating the pipe diffusion in austenite matrix. The alloy exhibited mixed ductile and intergranular mode of fracture in the entire temperature range. Few grains exhibited transgranular quasi-cleavage facets in the DSA range.

Keywords Ni-base superalloy · Superni 263 · Tensile properties · Dynamic strain ageing · Fracture

Introduction

The wrought Alloy 263 derives its strength by combined effects of solid solution and precipitation strengthening. The solid solution strengthening mainly results from elements such as Mo through lattice distortion, curtailing diffusion and by the reduction in stacking fault energy (SFE) (Smith et al. 2010; Gianfrancesco 2017). Additionally, intragranular γ' [Ni_3(Ti, Al)] contributes to its matrix strength, whereas precipitation of intergranular $M_{23}C_6$ on ageing promotes high-creep resistance at elevated temperatures. The alloy has been used in gas turbine engines in various components, and now, it is under consideration for usage in A-USC power plants which will operate at very high temperatures. The recent investigations have indicated that alloy-263 possessed better creep-rupture strength than the currently being considered candidate alloy, Inconel 617 for A-USC applications and lies very close to that of Nimonic 740 which is the other contender (Maile 2013). Alloy 263 is being produced under various trade names as C-263, Nimonic 263, Haynes 263 and Superni 263 (Jadav et al. 2019; Zhao et al. 2001).

Evaluation of tensile deformation behavior, work hardening rate and drawability characteristics of sheet material of 1 mm and 0.5 mm thickness, at room temperature was reported by Ankamma et al. (2011a, b). Tensile fracture studies of C-263 alloy under solutionized and different ageing conditions were investigated by Wanga et al. (2009). Serrated flow in 263 superalloy, at the intermediate temperature range (473–1033 K), and at a of 4×10^{-4} S^{-1}, was reported by Han et al. (Han et al. 2015). Volume fraction of γ' and ageing time were reported to exert major influence on tensile deformation behavior of 263 superalloy (Han et al. 2015; Wang et al. 2016; Cai et al. 2017). However, the effects of DSA on tensile properties as a function of strain rate and temperatures have not been explored so far. Therefore, this investigation is aimed at understanding the effects of strain rate, temperature, DSA on tensile properties, deformation and fracture behavior of Superni 263 superalloy over a temperature range of 298–923 K.

✉ K. V. Rajulapati
kvrse@uohyd.ernet.in; kvrse.uoh@gmail.com

[1] School of Engineering Sciences and Technology, University of Hyderabad, Hyderabad 500046, India

[2] Pratt & Whitney Chair, University of Hyderabad, Hyderabad 500046, India

[3] Defence Materials Stores R&D Establishment, Kanpur 208013, India

Experimental

The cylindrical samples of size (Φ 10 mm × 65 mm length) were machined from Φ70 mm solution annealed, rolled bars using electro-discharge machining. Superni 263 alloy was subjected to a heat treatment comprising of solutionizing (1373 K/90 min + water quenching) and ageing (1073 K/8 h + air cooling). The chemical composition of the alloy is given in Table 1. The tensile samples were machined as per the profile recorded in Fig. 1. Tensile testing has been conducted as per ASTM E 8 M and E21 standards (ASTM 2005a, b). Testing of the alloy was carried out in a computer controlled, screw-driven INSTRONc4500 series universal testing machine equipped with resistance heating furnace. The temperature during the test was monitored using K-type thermocouple tied on the gage portion of the specimen. All high temperature tensile tests were conducted after an equilibration for 15 min at the testing temperature. The tensile tests were conducted at strain rates of 1.3×10^{-2} S^{-1}, 1.3×10^{-3} S^{-1} and 1.3×10^{-4} S^{-1} at various temperatures (298–923 K). The fracture analysis of tensile tested samples was carried out using SEM (HITACHI S-3400 N) operating at an accelerating voltage of 15 kV.

Table 1 Chemical composition of Superni 263 superalloy (Balance-Ni)

Element	wt%	Element	wt%
C	0.074	**N**	0.005
Cr	20.00	**Mn**	0.400
Co	19.30	**Si**	0.030
Mo	05.90	**Ag**	0.0003
Ti	02.10	**B**	0.0050
Al	0.510	**Bi**	0.0005
P	0.005	**Pb**	0.0002
Fe	0.050	**S**	0.005
O	0.0012	**Cu**	0.020

Results

Microstructural Details

The solution annealing at 1373 K/1.5 h has dissolved a majority of the preexisting (Ti, Mo)C and (TiC) particles and led to the complete dissolution of chromium-rich $M_{23}C_6$ type of carbides and gamma prime (γ'). Average grain size of Superni 263 alloy determined through linear intercept method was ~ 160 µm. In the solution annealed state, the intragranular regions contained few annealing twins. Subsequent ageing at 1073 K/8 h caused the re-precipitation of Cr-rich complex $M_{23}C_6$ type of carbides on the grain boundaries and uniformly distributed spherical γ' in the intragranular locations. The average size of γ' was found to be 22 ± 5 nm. The 1073 K/8 h ageing treatment was found to give the optimum yield and tensile strengths.

Tensile Properties

The engineering tensile stress–strain curves of Superni 263 alloy are shown in Figs. 2(a–d) and 3(a–c) at various temperatures for three different strain rates. The 0.2% yield stress (YS), ultimate tensile strength (UTS) and ductility (% elongation) deduced at various strain rates and temperatures are shown in Fig. 4. The normalized work hardening rate (θ) of the alloy at different strain rates and temperatures is computed with the following expression:

$$\theta = \left[\frac{(\sigma_{0.05} - \sigma_{0.005})}{0.045}\right]/E;$$

where $\sigma_{0.05}$ and $\sigma_{0.005}$ are true stress values matching with true plastic strains 0.05 and 0.005, respectively. Figure 4d

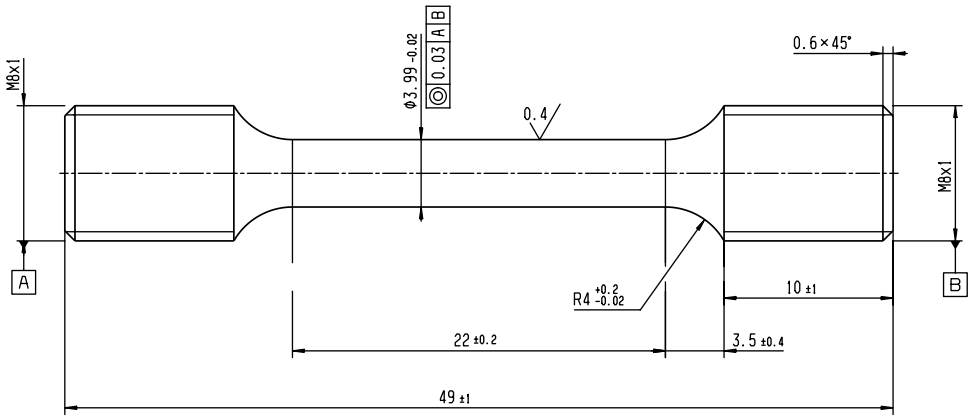

Fig. 1 Line diagram of tensile specimen adapted in the present study

shows the variation of (θ), with temperatures at the three different strain rates employed. The salient features from Fig. 4 include the following: (i) serrated flow occurred between 473 K and 923 K irrespective of the strain rate (Figs. 2 and 3) (ii) YS showed a peak at different temperatures depending on strain rate (Fig. 4a) (iii) the maximum YS occurred at 673 K at a $\dot{\varepsilon}$ of 1.3×10^{-3} S^{-1} (iv) YS decreased until 773 K followed by a plateau between 873 and 923 K at a $\dot{\varepsilon}$, 1.3×10^{-2} S^{-1} (v) plateau in YS shifted to lower temperatures at $\dot{\varepsilon}$, 1.3×10^{-4} S^{-1} (vi) there was a rapid fall in UTS with increasing temperature up to 873 K at 1.3×10^{-2} S^{-1} (Fig. 4b) (vii) two peaks were observed in UTS in its temperature dependence at 673 K and 873 K at a $\dot{\varepsilon}$ of 1.3×10^{-3} S^{-1}, whereas a single peak was displayed at 873 K at 1.3×10^{-4} S^{-1} (viii) a fairly high elongation was displayed by the alloy at 773 K irrespective of the $\dot{\varepsilon}$ (Fig. 4c) (ix) above 773 K, a rapid decrease in elongation was noticed at all the strain rates (x) the elongation minima was found at 1.3×10^{-3} S^{-1} in the range 573–673 K (xi) though the normalized work hardening rate (Fig. 4d) has not shown a systematic trend on temperature dependence, in general, the alloy exhibited higher rate at intermediate strain rate in the range 473–923 K. Higher work hardening rates are exhibited by the alloy at intermediate strain rate (1.3×10^{-3} S^{-1}), when compared to other strain rates employed.

Strain Rate Sensitivity

One of the prime manifestations of DSA is negative strain rate sensitivity (m) (Penning 1972), where *m* can be defined as variation in flow stress with strain rate, at a constant strain and temperature.

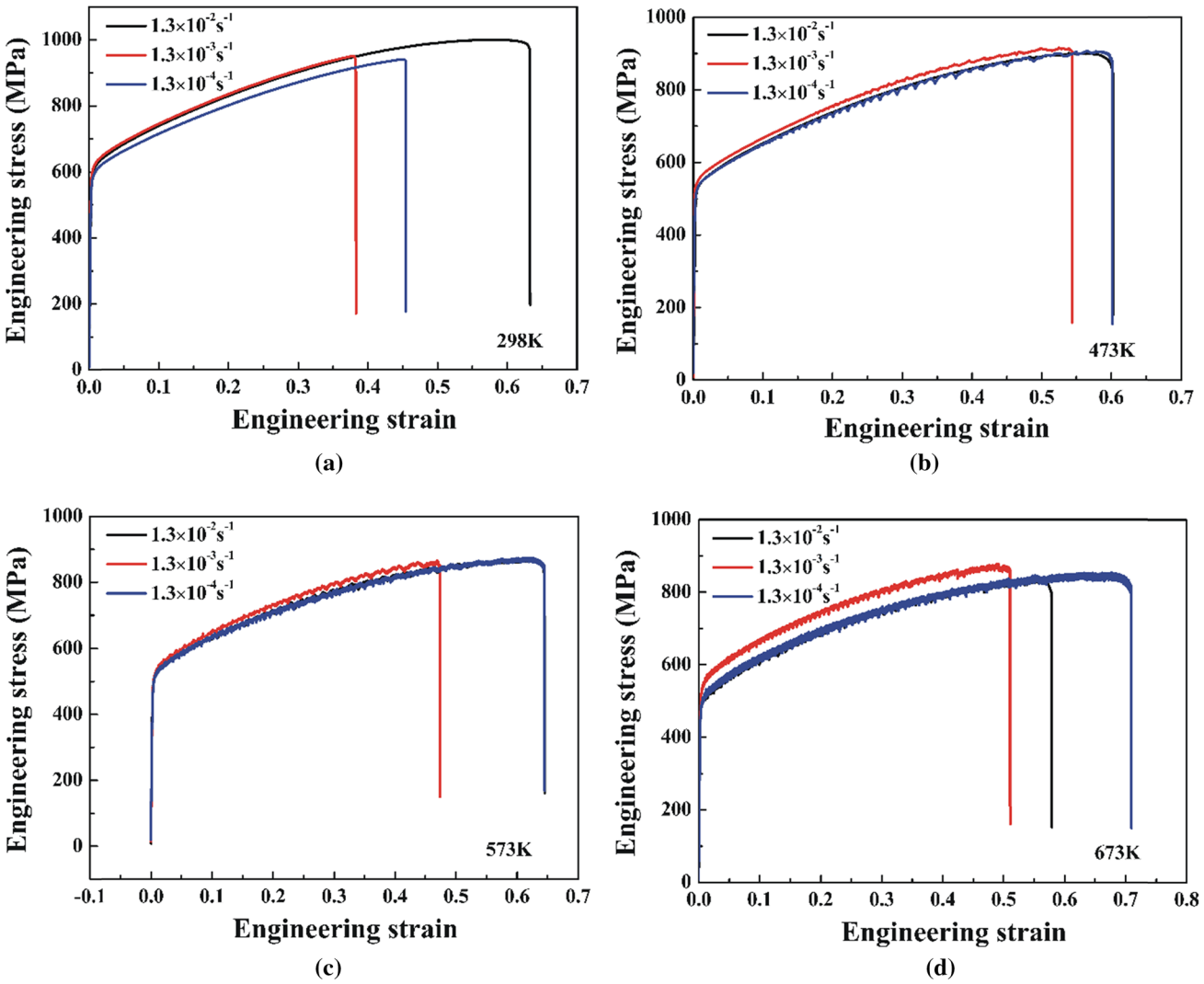

Fig. 2 Stress–strain plots of Superni 263 alloy at different strain rates in the temperature regime (298–673 K)

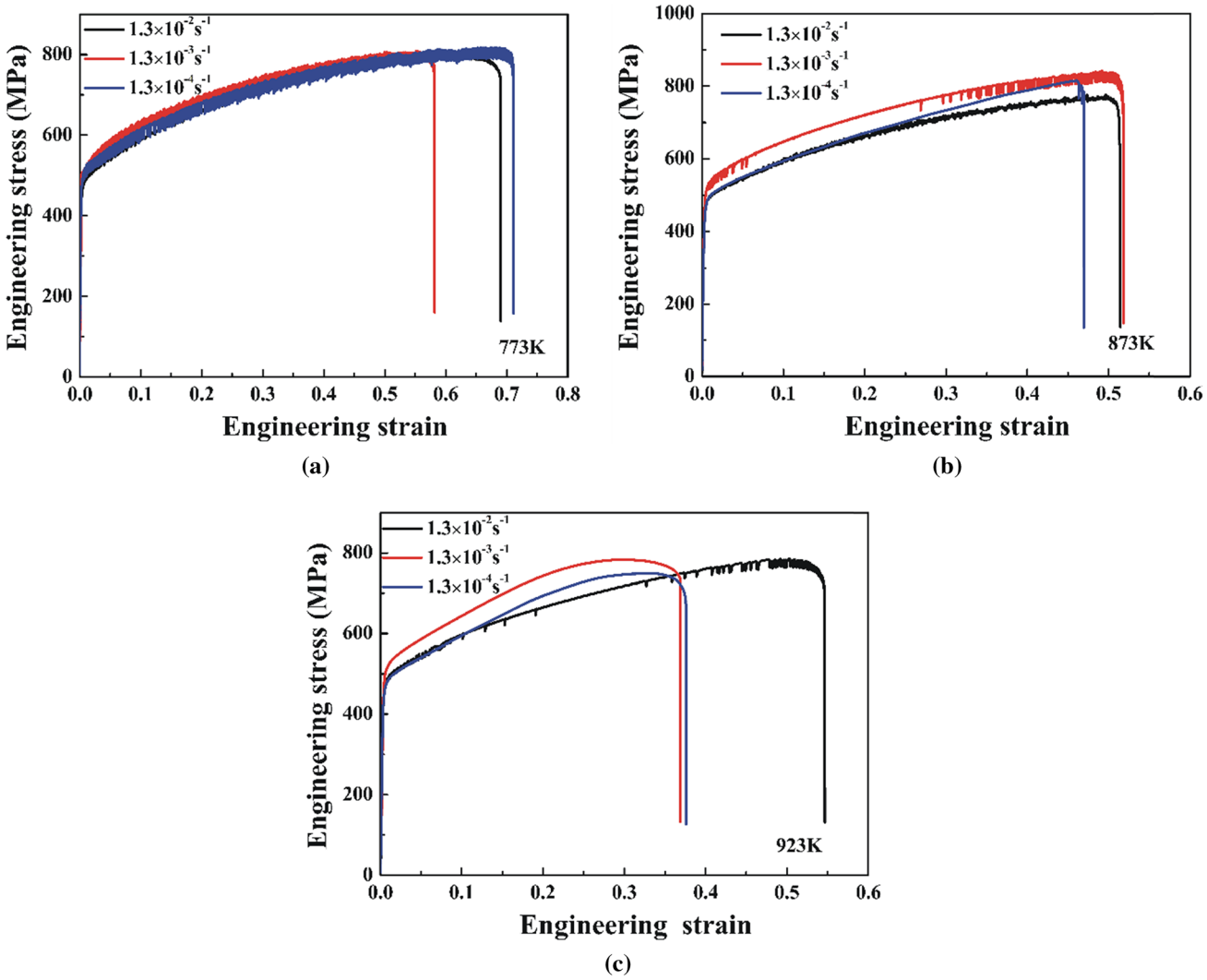

Fig. 3 Stress–strain plots of Superni 263 alloy at different strain rates in the temperature regime (773–923 K)

$$m = \frac{\log\left(\frac{\sigma 2}{\sigma 1}\right)}{\log\left(\frac{\dot{\varepsilon} 2}{\dot{\varepsilon} 1}\right)} |\varepsilon, T$$

where σ_2, σ_1 are the flow stresses at strain rates, respectively. The alloy has exhibited positive m value at 298 K and negative m values in the temperature range of 473–923 K, where m values are determined at 4% plastic strain.

Serrated Flow

The representative true stress–true strain plots of Superni 263 alloy, obtained in the temperature range of 298–923 K at three different strain rates (1.3×10^{-3} s^{-1}, 1.3×10^{-4} s^{-1}, 1.3×10^{-5} s^{-1}), are shown in Fig. 5. At all the strain rates, the room temperature stress–strain curves remained smooth and no serrations were seen. Various types of serrations (types A, A + B and C) were observed depending on temperature and strain rate combinations. The classification of the type of serrations was as per the scheme proposed in (Rodriguez 1984). Serrated flow was generally found to occur after a certain amount of plastic deformation. The plastic strain associated with the formation of first serration in the true stress–strain curves was defined as a critical strain (ε_c). The lower temperature for the onset of serrated flow at all the three strain rates was found to be 473 K. The upper temperature for the appearance of serrated flow increased with increasing strain rate; the upper temperature was found to be 773 K, 873 K and 923 K for strain rates of 1.3×10^{-4} S^{-1}, 1.3×10^{-3} S^{-1} and 1.3×10^{-2} S^{-1}, respectively. There has been a shift for the occurrence of type C serrations to lower temperatures with decreasing strain rate. Similar observations were found earlier

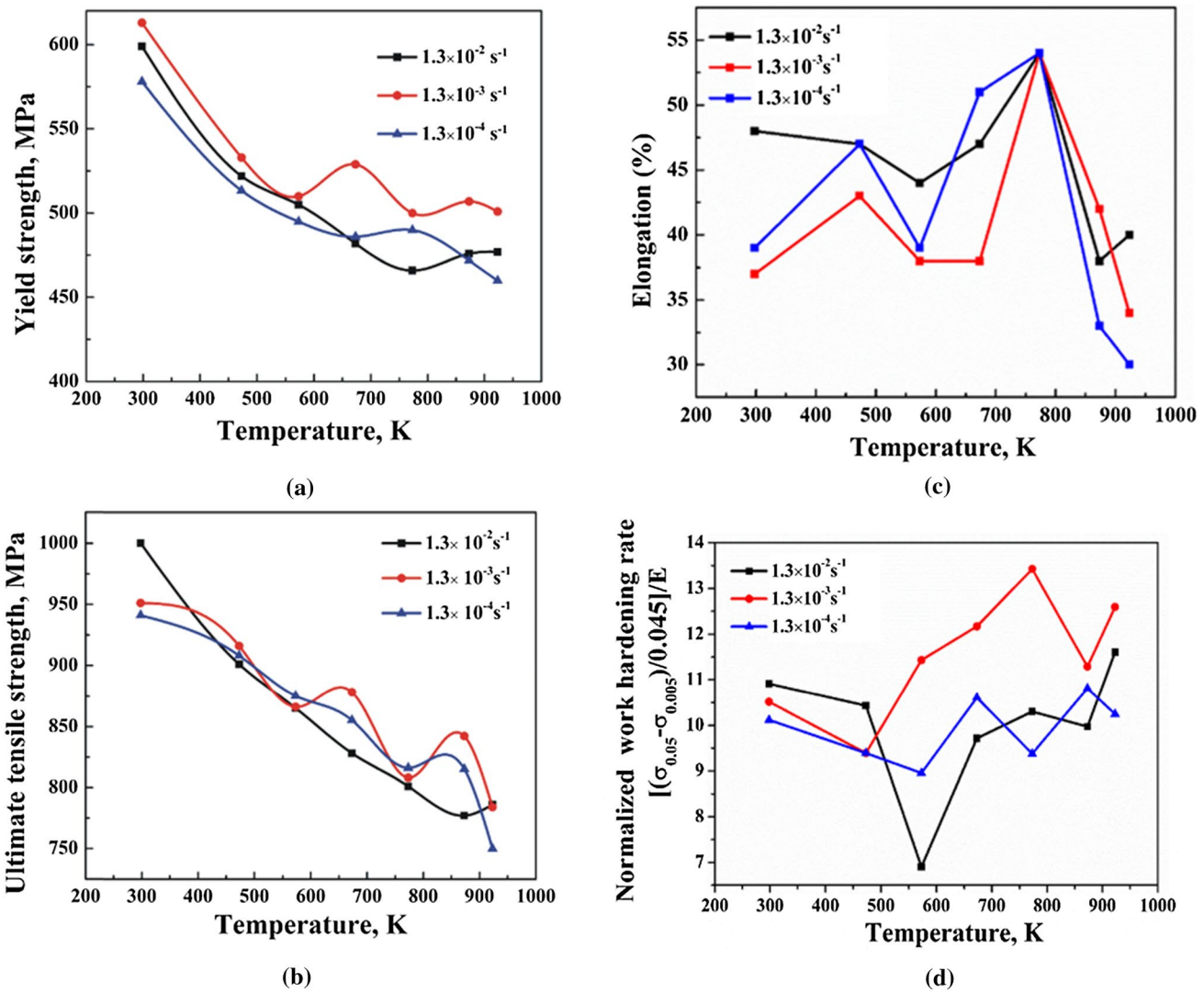

Fig. 4 Variation of **a** yield strength, **b** ultimate tensile strength, **c** percentage elongation and **d** normalized work hardening rate as a function of temperature and strain rate

in precipitation strengthened superalloy Nimonic PE16 (Bhanu Sankara Rao et al. 1986). The magnified view of most prominent serrated flow regime clearly revealed the type of serrations (Fig. 5b). Serrations that appeared at lower temperatures could be classified as type A or type (A + B), while type C prevailed at high temperatures at all the three strain rates. The details pertaining to the range of temperatures and strain rates that describe the presence of different types of serrations are incorporated in Fig. 6. The ε_c varied as a function of strain rate and temperature (Fig. 6). The ε_c decreased with rise in temperature and decreasing strain rate when the serrations were type A and A + B. This behavior has been generally acknowledged as normal PLC effect (Penning 1972; Cottrell 1953). In the temperature range where type C serrations were found, the ε_c increased with decreasing strain rate, which was recognized as inverse PLC effect (Brechet and Estrin 1995).

The activation energy for serrated flow could be determined by the expression proposed by McCormick (1972) and Sleeswyk (1958) in the temperature range where normal PLC was proposed to occur. The following equation was derived for accounting the static ageing models of DSA.

$$\varepsilon_c^{m+\beta} = [(\mathrm{C1}/\alpha \mathrm{Co})^{3/2} \dot{\varepsilon} \mathrm{kTbexp}\left(Q_\mathrm{m}/\mathrm{kT}\right)]/[3LN_d K_\mathrm{v} U_\mathrm{m} D_\mathrm{o}];$$

where C_1 is the solute concentration at dislocation needed to lock it, C_o is the original concentration of the alloy, α is a constant, Q_m is the activation energy for solute migration, L is the obstacle spacing, U_m is the binding energy between solute and dislocation, D_o is the pre-exponential coefficient

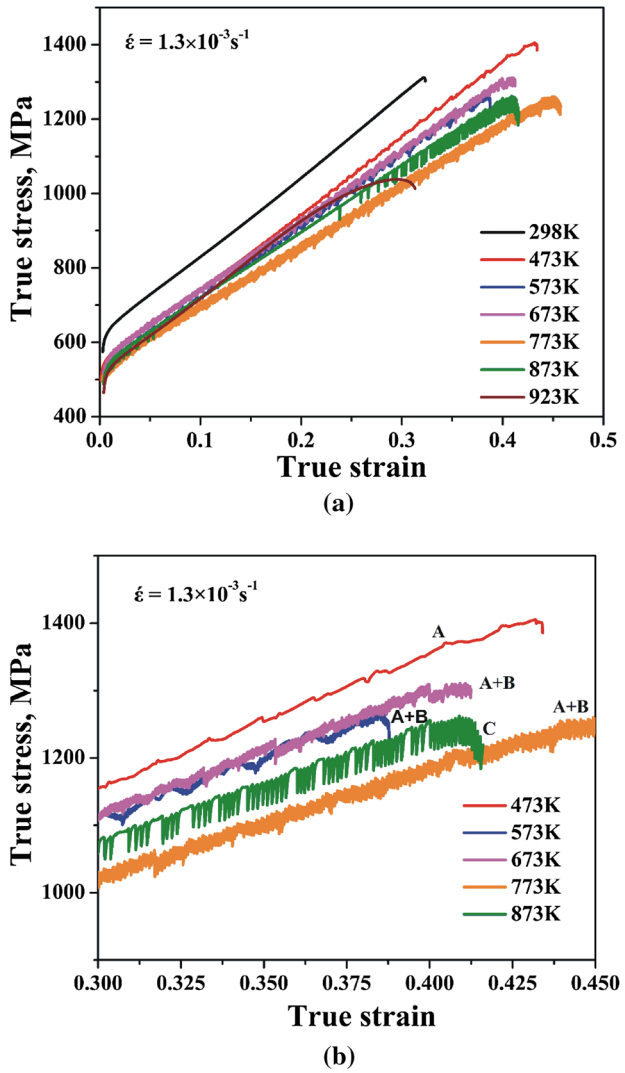

Fig. 5 **a** Temperature dependence of flow stress at a strain rate of 1.3×10^{-3} S^{-1} and **b** the corresponding magnified view of serrated flow

in the relationship $\left(D = D_o \exp\left(-\frac{Q_m}{kT}\right)\right)$; where D is the diffusion coefficient, k is the Boltzmann constant, T is the temperature, and b is the Burgers vector. The parameters K_v, m, N_d and β are related to the strain dependence of vacancy concentration C_v and mobile dislocation density ρ_m by $(C_v = K_v\varepsilon^{\beta})$; $(\rho_m = N_d\,\varepsilon^{m})$; $(\rho_m = N_d\varepsilon^{\beta})$; Slope $(m+\beta)$ was deduced from the plots of ln $(\dot{\varepsilon})$ and ln (ε_c) at 573 K and 773 K (Fig. 7). In the current study, the $(m+\beta)$ value obtained is ~ 1.4 at 573 K and 773 K. Q is evaluated from a plot of ln (ε_c) vs $1/T$, at a particular strain rate $\left(Q = \left(\text{slope of ln } \varepsilon_c \text{vs } 1000/T \text{ plot}\right) \times (m+\beta) \times 1000 \times k\right)$. The estimated Q values for type A and A + B serrations are in the range 68–77 kJ/mol.

Fracture Behavior

Detailed investigations performed on fracture surfaces of the failed samples indicated a mixed mode fracture. In general, the fracture surfaces were predominantly endowed with dimples which are known to result as a consequence of microvoid coalescence in the transgranular regions. At few places, the intergranular cracks were seen in the locations where the transgranular quasi-cleavage facets prevailed. Figure 8 illustrates these features at different temperatures for a strain rate of 1.3×10^{-3} s^{-1}.

Discussion

Serrated Flow and Dynamic Strain Ageing

The serrated flow has often been attributed to dynamic interaction of either interstitial or substitutional solute atoms with deformation-induced mobile dislocations which is considered as DSA (Choudhary 1999). The temperature and strain rate combinations decide the type of solute atoms that are responsible for DSA. In the temperature zone representing A and A + B serrations, the critical strain decreased with increasing temperature at all the three strain rates. The apparent activation energy for the discontinuous yielding in the normal PLC regime was found to be in the 68–77 kJ/mol (Fig. 7). This value compares well with that reported for Nimonic Alloy 263 (Han et al. 2015) and corresponds to the pipe diffusion of Cr and Mo in austenite matrix. This observation reveals that the serrated flow in the low temperature regime results from the locking of mobile dislocations by substitutional solute atmospheres. The temperature for the formation of Type C serrations increased with increasing strain rate (Fig. 6a). The critical strain for the occurrence of type C serrations increased with increasing temperature and decreasing strain rate (Fig. 6b). It was generally presumed that the type C serrations would result from the detachment of dislocations from the already prevailing substitutional solute atmospheres (Koul and Pickering 1982; Jenkins and Smith 1969). The occurrence of type C serrations has also been reported to result from the repeated shearing of gamma prime particles by the dislocations moving in parallel slip bands pertaining to the same slip system (Doi and Shimanuki 1972). In this investigation, the Superni 263 alloy was examined in the peak-aged state and the tensile testing at elevated temperatures resulted in the deformation substructure comprising of very short planar slip bands, very high dislocation density represented by tangles, dipoles, loops and dislocation pairs within the grains. In spite of the persistence of the gamma prime shearing, the stress–strain curves of Superni 263 remained smooth and did not display type C serrations at temperatures higher than 873 K at the two lower

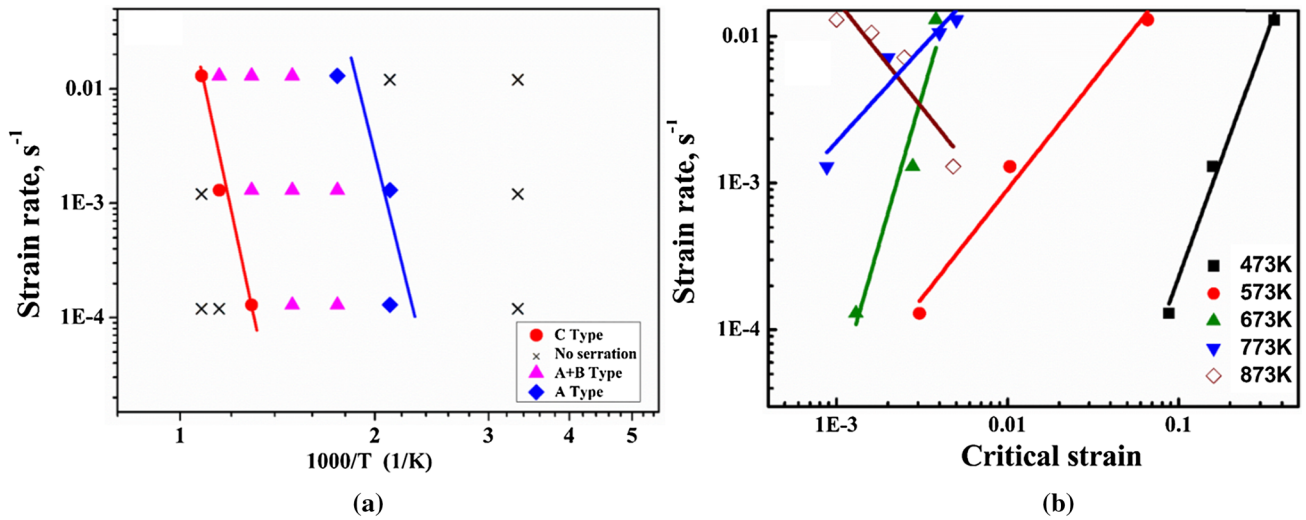

Fig. 6 **a** Details of serrated flow in Superni 263 alloy at different temperatures and strain rates and **b** variation of critical strain as a function of strain rates and temperatures

strain rates, i.e., 1.3×10^{-3} S^{-1} and 1.3×10^{-4} S^{-1} (Fig. 5). These observations clearly indicate that shearing of gamma prime is not responsible for evolution of type C serrations during tensile tests.

Tensile Properties

In the superalloys containing a higher volume fraction of gamma prime, the YS and UTS have been noticed to increase with raise in tensile testing temperature initially, displaying a maximum at an intermediate temperature followed by rapid fall at very high temperatures. This type of behavior has been attributed to the following: (i) increase in the order of gamma prime particles that contribute to the intrinsic strength of gamma prime with raise in temperature (Pope and Ezz 1984) and (ii) to the movement of screw dislocations by cross-slip from the (111) planes where they are mobile to the (010) planes where they become immobile (Gianfrancesco 2017). On the other hand, the low volume fraction gamma prime hardened alloys such as Nimonic PE 16 did not reveal the strength increase with the initial raise in temperature at higher strain rate (Bhanu Sankara Rao et al. 1986). Superni 263 is a low gamma prime volume fraction alloy, and its temperature-dependent strength properties at high strain rates (Fig. 4) are similar to those seen in Nimonic PE16 superalloy at higher strain rate.

In general, the peaks and plateaus in YS and UTS in several commercial steels and superalloys have been reported to result from the DSA effects at lower strain rates (Rodriguez 1984; Bhanu Sankara Rao et al. 1986; Choudhary 1999; Shankar et al. 2004; Gopinath et al. 2009). In case of Superni 263 superalloy, the influence of DSA is more pronounced at strain rate of 1.3×10^{-3} S^{-1} as depicted by the peaks in YS and UTS values (Fig. 4). The engineering stress–strain curves shown in Figs. 2 and 3 for three strain rates at different temperatures clearly elucidate the negative strain rate dependence of flow stress in the range 473–923 K. The existence of the negative strain rate sensitivity is a clear manifestation for the occurrence of DSA in the range 473–923 K. This observation suggests that the DSA occurs over a wide temperature range though it may not reveal the signatures of serrated flow certain times.

Superni 263 alloy showed lower values of elongation in the temperature range where the negative strain rate sensitivity was predominantly observed (Fig. 9). This observation points to the involvement of DSA in lowering the ductility. This can be understood based on the dislocation generation and their re-arrangements that can occur in the DSA regime. It has been pointed out earlier that DSA leads to immobilization of dislocations by solute atmospheres. However, the progression of tensile test calls for continuous generation of dislocations at the imposed strain rate. Several investigations considered that DSA promotes dislocation multiplication rapidly and leads to delay in the occurrence of recovery which manifests in the form of cells (Dingley and Mclean 1967; Garde et al. 1972; Morris 1974; Mannan et al. 1982). As a result, in many alloys, the dislocation density was shown to be high and more homogenously distributed. The pinning of dislocations locally retards the dislocation recovery giving rise to more uniform dispersion (Embury 1971). Consistent with the above observations, Superni 263 superalloy in this study also displayed very high density of dislocations with more uniform distribution in the DSA domain. The absence of cells in the substructure could be treated as an evidence for solute segregation and inability of screw dislocations to cross-slip due to reduced mobility

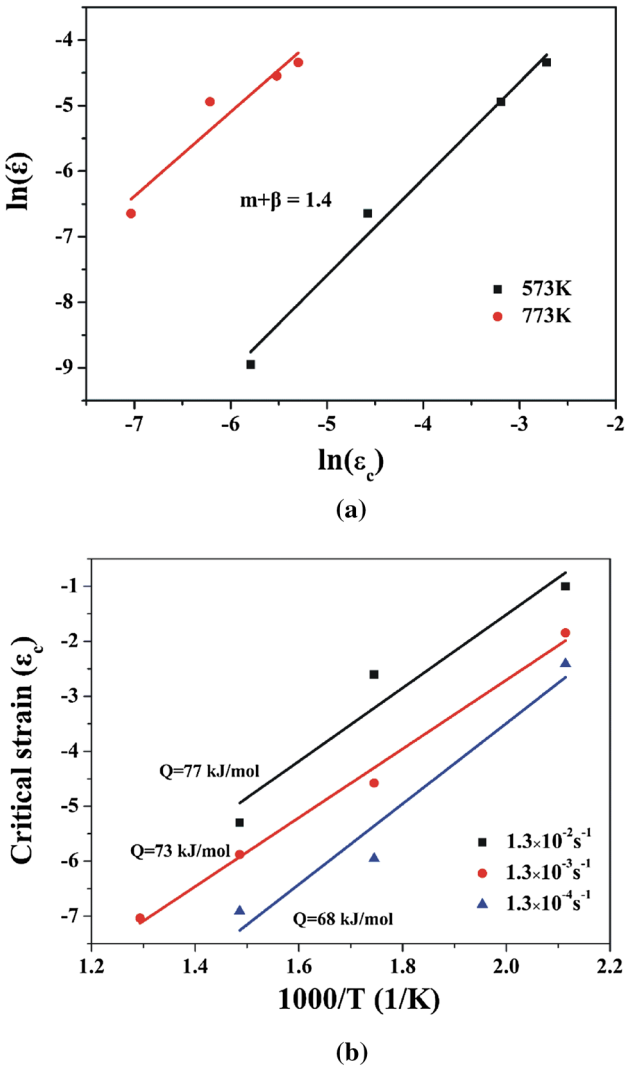

Fig. 7 Determination of activation energy. **a** Plot of ln (ε_c) *vs* ln($\dot{\varepsilon}$). **b** Plot of 1/*T* *vs* critical strain

(Hornbogen 1964; Hirth 1982). The low uniform elongation in the DSA range could arise from the factors mentioned above. The maximum in ductility as displayed by percentage elongation at fracture was seen at 773 K irrespective of the strain rate (Fig. 4c). This observation is corroborated by the peak in work hardening rate at 773 K for a strain rate of 1.3×10^{-3} S^{-1} (Fig. 4d). The alloy showed a rapid fall in elongation above 773 K (Fig. 4c). It appears that the strength generated in the matrix due to DSA can be quiet high, and in the vicinity of grain boundary, this may exceed the cohesive strength between the grain boundaries and the carbides located on them. The microcracks on the grain boundaries could result from the de-cohesion of interface between the intergranular $M_{23}C_6$ particles and grain boundary. These microcracks in turn join and become a major intergranular crack. The transgranular quasi-cleavage facets appear to result from the channelization of deformation in the planar slip bands. The increased proportion of intergranular cracking in the mixed mode fracture contributes to the rapid fall in elongation at very high temperatures.

Conclusions

- The tensile properties of Superni 263 superalloy were found to be a complex function of temperature and strain rate. The alloy exhibited plateaus and peaks in yield and tensile strength values in its temperature dependence. The temperature at which the peak strength was observed was dependent on strain rate.
- In general, the alloy exhibited high strength values at a strain rate of 1.3×10^{-3} S^{-1} in the range 298–923 K. The peak in yield strength was seen at 673 K.
- The stress–strain behavior of the alloy was characterized by the occurrence of serrated flow at temperatures higher than 473 K. The maximum temperature where the serrated flow found to occur was dependent on strain rate. At a strain rate of 1.3×10^{-2} S^{-1}, serrated flow prevailed in the range 473–923 K, while at 1.3×10^{-3} S^{-1} and 1.3×10^{-4} S^{-1}, the serrated flow range was noticed to be 473–873 K and 473–773 K, respectively. Serrated flow in plastic deformation regime is considered as one of the manifestations of dynamic strain ageing.
- The serration types and the critical strain for the onset of serrations varied as a function of temperature and strain rate. The serrations observed are type A and A + B at low temperatures and C at high temperatures. The critical strain decreased with increasing temperature and decreasing strain rate in conditions where type A and A + B serrations were found. The activation energy for the occurrence of serrated flow was found to be 68–77 kJ/mole which is in conformity with the pipe diffusion of substitutional solute atoms in austenite matrix.
- Alloy exhibited negative strain rate sensitivity in flow stress in the range 473 K to 923 K indicating the operation of DSA.

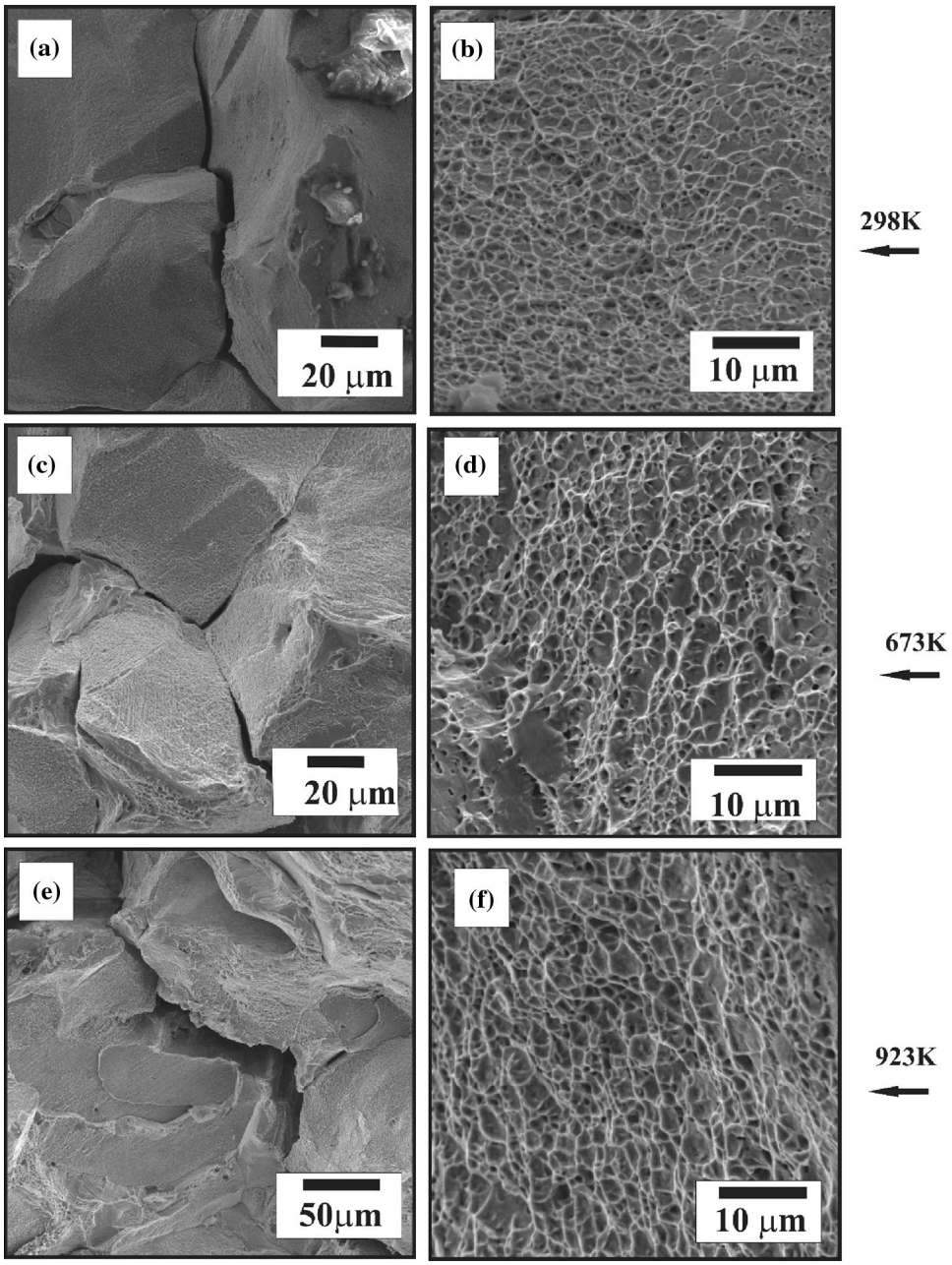

Fig. 8 Fractographs of samples tested at a $\dot{\varepsilon}$ of 1.3×10^{-3} S^{-1} and at **a**, **b** 298 K, **c**, **d** 673 K and **e**, **f** 923 K

- The alloy displayed a very high work hardening rates in the DSA regime at strain rate of 1.3×10^{-3} S^{-1}. The ductility was found low in the DSA range. The alloy exhibited mixed ductile and intergranular mode of fracture in the entire temperature range. Few grains exhibited transgranular quasi-cleavage facets in the DSA range.

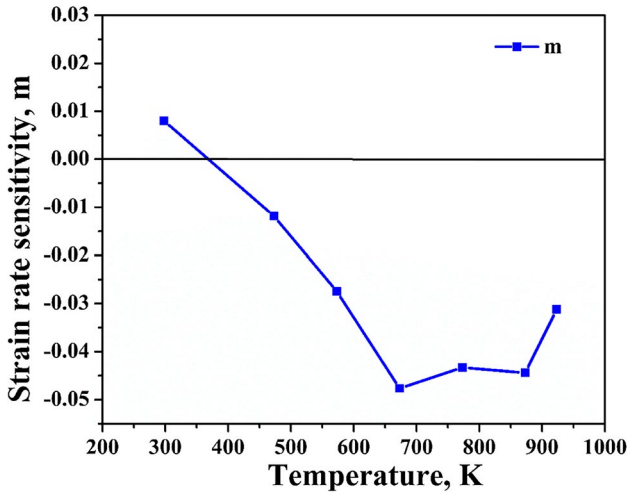

Fig. 9 Variation of strain rate sensitivity of Superni 263 alloy with temperature at 4% true plastic strain

Acknowledgements The authors gratefully acknowledge DST-PURSE and DST-FIST programs of School of Engineering Sciences and Technology, University of Hyderabad for providing some of the experimental facilities used in this investigation.

References

Ankamma K et al (2011a) Effect of aging on work hardening behavior of cold rolled Nimonic C-263 alloy. Mater Sci Technol 27:1333–1340

Ankamma K, Satyanarayana DVV, Chandramohan Reddy G, Komaraiah M, Eswara Prasad N (2011b) In-plane anisotropy in tensile deformation and its influence on the drawability of Nimonic C–263 alloy sheets. SADHANA Acad Proc Eng Sci 36:223–249

ASTM E 8M-04 (2005a) Standard test methods for tension testing of metallic materials, vol 3.01. ASTM International, West Conshohocken, pp 86–109

ASTM E 21-03a (2005b) Standard test methods for elevated temperature tension tests of metallic materials, vol 3.01. ASTM International, West Conshohocken, pp 150–157

Bhanu Sankara Rao K, Seetharaman V, Mannan SL, Rodriguez P (1986) Strain rate and temperature dependence of formation and fracture behavior of a Nimonic PE16 Superalloy. High Temp Mater Process 7:63–81

Brechet Y, Estrin Y (1995) On the influence of precipitation on the Portevin-Le Chatelier effect. Acta Metall Mater 43:955–963

Cai Y, Tian C, Zhang G, Han G, Yang S, Fu S, Cui C, Zhang Q (2017) Influence of γ' precipitates on the critical strain and localized deformation of serrated flow in Ni-based superalloys. J Alloys Compd 690:707–715

Choudhary BK, Bhanu Sankara Rao K, Mannan SL, Kashyap BP (1999) Serrated Yielding in 9Cr-1Mo ferritic steel. Mater Sci Technol 15:791–797

Cottrell AH (1953) A note on the Portevin-Le Chatelier effect. Philos Mag 44:829–832

Dingley DJ, Mclean D (1967) Components of flow stress of Iron. Acta Metall 15:885–901

Doi H, Shimanuki Y (1972) In: Proceedings of 2nd international conference on superalloys-processing, Champion, Pennsylvania

Embury JD (1971) Strengthening methods in crystals. Wiley Publishers, New York, p 331

Garde AM, Santhanam AT, Reed-Hill RE (1972) Acta Metall 20:215

Gianfrancesco AD (2017) Materials for ultra-supercritical and advanced ultra-supercritical power plants. Elsevier, New York, p 571

Gopinath K, Gogia AK, Kamath SV, Ramamurty U (2009) Dynamic strain aging in Ni based superalloy 720Li. Acta Mater 57:1243–1253

Han GM, Tian CG, Chu ZK, Cui CY, Hu ZQ, Sun XF (2015) Activation energy calculations for the Portevin–Le Chatelier effect in nimonic 263 superalloy. Metall Mater Trans A 46:4629–4635

Hirth JP (1982) In: Meshii M (ed) Mechanical properties of BCC metals, vol 181. TMS, Warrendale, PA, pp 181–187

Hornbogen E (1964) Trans ASM 57:122–132

Jadav J, Rajulapati KV, Bhanu Sankara Rao K, Eswara Prasad N, Mythili R, Prasad K (2019) Strain controlled isothermal low cycle fatigue life, deformation and fracture characteristics of Superni 263 superalloy. Mater Sci Eng A 760:296–315

Jenkins CF, Smith GV (1969) Serrated plastic flow in austenitic stainless steel. Trans TMS-AIME 245:2149–2156

Koul AK, Pickering FB (1982) Serrated yielding in Ni-Fe base superalloys at 700°C. Scripta Met 16:119–124

Maile K (2013) Qualification of Ni-based alloys for advanced ultra supercritical plants. Proc Eng 55:214

Mannan SL, Samuel KG, Rodriguez P (1982) In: Giffkins RC (ed) Proceedings of 6th international conference on strength of metals and alloys, p 637

McCormick PG (1972) A model for the Portevin-Le Chatelier effect in substitutional alloys. Acta Metall 20:351

Morris JG (1974) Dynamic strain aging in aluminium alloys. Mater Sci Eng 13:101–108

Penning P (1972) Mathematics of the Portevein-Le Chatelier effect. Acta Metall 20:1169–1175

Pope DP, Ezz SS (1984) Int Mater Rev 29:136

Rodriguez P (1984) Serrated plastic flow. Bull Mater Sci 6:653–663

Shankar V, Valsan M, Bhanu Sankara Rao K, Mannan SL (2004) Effects of temperature and strain rate on tensile properties and activation energy for dynamic strain aging in alloy 625. Metall Mater Trans A 35:3129–3139

Sleeswyk AW (1958) Slow strain-hardening of ingot iron. Acta Metall 6:598–603

Smith SA, West GD, Chi K, Gamble W, Thomson RC (2010) Advances in materials technology for fossil power plants. In: Proceedings from 6th international conference, pp 110–126

Wang X, Han G, Cui C, Guan S, Jin T, Sun X, Hu Z (2016) The dependence of Portevin–Le Châtelier effect on the γ' precipitates in a wrought Ni-Base Superalloy. Metall Mater Trans A 47:5994–6003

Wanga WZ, Honga HU, Kima IS (2009) Influence of and grain boundary carbide on tensile fracture behaviours of Nimonic 263. Mater Sci Eng A 523:242–245

Zhao JC, Ravikumar V, Beltran AM (2001) Phase precipitation and phase stability in Nimonic 263. Metall Mater Trans A 32:1271–1282